Title

Energy and power quality measurement for electrical distribution in AC and DC microgrid buildings

Authors

Gerber, Daniel L

Ghatpande, Omkar A

Nazir, Moazzam

et al.

Publication Date

2022-02-01

DOI

10.1016/j.apenergy.2021.118308

Peer reviewed

Energy and Power Quality Measurement for Electrical Distribution in AC and DC Microgrid Buildings

Daniel L. Gerber[a,*], Omkar A. Ghatpande[b], Moazzam Nazir[b], Willy G. Bernal Heredia[b], Wei Feng[a], Richard Brown[a]

[a]*Lawrence Berkeley National Laboratory, Building 90, 1 Cyclotron Rd, Berkeley, CA 94720*
[b]*National Renewable Energy Laboratory, 15013 Denver W Pkwy, Golden, CO 80401*

Abstract

Today's selection of DC microgrid buildings features a diverse set of electrical topologies and turnkey solutions, each with specific design trade-offs and optimizations. Designers desperately need standardized metrics and procedures for measurement and verification (M&V) to analyze and compare the advantages of each DC solution to traditional AC building networks. This work develops M&V procedures for quantifying and comparing the energy efficiency and power quality in buildings. To calculate full-building efficiency, this work introduces the measurement-informed modeling method, a procedure that develops and refines a building's energy model with metered data. To quantify power quality, this work defines a new voltage quality index that applies to both AC and DC buildings. This article describes the equipment, instrumentation, and operation necessary to calculate the efficiency and power quality. It then demonstrates these methods with a set of field tests. These M&V procedures can ultimately be used to compare and improve the efficiency and power quality of various DC topologies.

Keywords: DC microgrids, buildings, measurement and verification, energy, power quality

1. Introduction

1.1. DC Microgrid Buildings

Many types of microgrid topologies have been developed to address the building sector's demand for resilience and clean energy. Among these, direct current (DC) microgrids have garnered support

*Corresponding author

Email addresses: dgerb@lbl.gov (Daniel L. Gerber), Omkar.Ghatpande@nrel.gov (Omkar A. Ghatpande), Moazzam.Nazir@nrel.gov (Moazzam Nazir), Willy.BernalHeredia@nrel.gov (Willy G. Bernal Heredia), weifeng@lbl.gov (Wei Feng), rebrown@lbl.gov (Richard Brown)

and academic interest due to a number of expected advantages over the traditional alternating current (AC) topologies. Most types of distributed energy resources are internally DC, including photovoltaic (PV) generation and battery storage. In addition, modern versions of most loads are internally DC, including electric vehicle (EV) charging, LED lighting, electronic equipment, and variable-speed brushless DC motors in heating, ventilation, air conditioning (HVAC), and refrigeration. DC distribution can reduce power conversion losses from DC to AC and back, allowing for across-the-board electrical savings. DC microgrids also have the potential for superior power quality. They often have a bidirectional gateway inverter that buffers the internal electrical networks from grid events. In addition, DC systems are usually devoid of 60 Hz harmonics and do not suffer from grid synchronization challenges.

Other potential advantages of DC include cost, resilience, safety, combined data and power, and the potential for managed power distribution. These advantages may also provide a strong value proposition and will be important to study in future work.

1.2. Energy Savings in DC Buildings

Over the past decade, many researchers have studied and analyzed the potential electrical savings with DC. These studies have reported a wide range of savings, from 2% [1] to as much as 19% [2]. Early works estimate the savings based on the conversion loss of typical systems [1–5]. These systems often include modeled conversion for the solar PV inverter, battery inverter, gateway inverter (a.k.a. grid-tie inverter), and any conversion at the load, including wall adapters and LED drivers. Later works develop more sophisticated side-by-side comparison studies and often use simulation tools to incorporate wire loss, converter efficiency curves, battery charging algorithms, and annual load profiles [6–9]. Current research examines ways in which to further improve analyses [10–12], which may include creating a detailed model of losses within the power converters themselves [13].

These studies all found DC to save the most electricity in buildings with a large PV and battery capacity. Buildings that generate most of their power can minimize the use of the gateway converter, reducing its conversion loss. Most of the efficiency studies assume the DC system has a simple bus-based architecture. However, many DC systems today feature an intricate network of power electronics and conversions. Although such systems certainly showcase the DC advantages in installation, safety, controls, and data, these benefits may come at the cost of efficiency.

Several past works use experiments to validate the efficiency savings in common DC systems. Some of these studies analyze the savings on a device-by-device basis. They often analyze and even rework end-use loads for DC input in order to study the savings potential of each device at scale [14–16]. Other studies develop a small-scale system level experiment with a limited set of end-use loads [17]. In general, a precise full-building efficiency study is very difficult. An experimental study involving a side-by-side AC and DC comparison would need to have identical solar, battery, and load profiles. Otherwise, the experiment would have to precisely meter the power within every load in the building—an impossible task. This work studies how modeling can help alleviate such metering requirements.

1.3. Power Quality in DC Buildings

Power quality studies a range of electrical issues that can affect a building or microgrid's power delivery, equipment health, and transmission loss. Several key standards currently exist for measuring power quality in AC systems, many of which may be appropriately applicable to DC buildings. IEEE Std 1159 details recommended practices for power quality measurement [18]. This standard describes all the major categories of power quality issues: transients, short-duration events (e.g., sags, swells, minor interruptions), long-duration events (over/under voltage, major interruptions), voltage unbalance, waveform distortion (harmonics, flicker), and frequency deviation. For each category, EN 50160 defines the limits of normal operating conditions for the network voltage in low- and medium-voltage systems [19]. Bus-voltage disturbances such as transients, sags, and swells may be detrimental to electronic equipment and must fall within the curves defined either by the Computer Business Equipment Manufacturers Association (CBEMA) or the Information Technology Industry Council (ITIC) [20]. Standards such as ANSI C84.1 place additional specifications on the supplier and device-side bus voltage levels [21]. Several standards limit the acceptable waveform distortion. Current harmonics at a building's point of common coupling are specified in IEEE-519 [22]. Device-side electromagnetic compatibility and harmonic limits are specified in IEC 61000-3-2 [23]. And finally, IEC 61000-3-3 [24] establishes acceptable limits on flicker, though eventually all LED drivers will be designed to cancel flicker.

Several recent articles have investigated power quality issues in DC systems [25–27]. Many of the DC power quality metrics are similar to their AC counterparts, but there are several key differences in classification. While the AC bus voltage refers to a root mean square (RMS) measurement, the

DC bus voltage is found through averaging. In addition, DC systems do not require metrics for frequency deviation or 60 Hz harmonics. They instead have an interharmonic metric that measures the waveform distortion due to switching converters on the bus. Although these works are comprehensive in describing the various power quality issues, they do not develop measurement procedures or methods of comparison.

Various past works have attempted to combine multiple power quality issues into a single metric. This metric is known in most works as the total power quality index (TPQI), though is also referred to as the global PQI or unified PQI. The TQPI provides a general sense of a site's power quality and has, thus far, only been defined for AC systems. Most works calculate the TPQI from submetrics related to eight power quality issues: long interruptions, short interruptions, frequency variation, harmonics, voltage unbalance, sags and swells, voltage variations, and flicker. The TPQI is the weighted sum of each submetric. Most methods calculate the submetrics based on how many times an event happens (e.g., number of interruptions in a year) or discrete tolerance bands (e.g., how many times frequency deviates outside the standard grid tolerance range of 59.7–60.3 Hz).

Early research quantified TPQI based on a simple set of metrics: voltage level, unbalance, flicker, and harmonics [28]. The voltage-level submetric was later qualified by sags, swells, and transients, based on the CBEMA [29] and ITIC curves [30]. Researchers have also studied the possibility of using cost metrics [31] or reliability metrics (e.g., system average interruption frequency index) [32]. Besides defining submetrics, many other previous works focus on how to weigh the submetrics in the TPQI calculation. The most popular method of weight calculation is via an analytical hierarchy process, which involves calculating a judgment matrix (a.k.a. Yager-Saaty matrix) [32–36]. The weights are the judgment matrix's maximum eigenvector. Other past works calculate the weights through a variety of other methods, including K-means clustering [37], grey clustering and entropy weight [38], and artificial neural networks [39].

Despite past research efforts to develop and calculate a TPQI, power quality continues to be an enigma among building and microgrid operators. Quantifying most submetrics requires specialized in-person M&V with expensive equipment. This work develops a new power quality index that simplifies and combines known power quality metrics as appropriate. It aims to lower the cost and complexity of measuring power quality, and its submetrics apply equivalently in AC and DC microgrids.

1.4. Motivation for M&V in DC Systems

DC microgrid buildings are being developed across the world, often as an experiment, demonstration, or statement piece. Today's DC topologies vary greatly depending on the manufacturer and region-specific building codes. Unlike for AC, DC developers and manufacturers lack a standardized design practice. Many DC companies develop their own all-in-one turnkey solutions. Although these solutions adhere to loose guidelines on voltage level (e.g., 48 V, 380 V), they are diverse in network topology and control protocol. Their allowable hardware and loads are often limited to partner companies. These companies will often prioritize a set of desirable qualities at the expense of others. For example, many smart-building solutions will trade-off electrical efficiency for improved controls and managed power distribution.

It is of utmost importance to develop metrics and M&V methods that can compare the various commercial DC systems amongst themselves and standard AC buildings. These analyses will contribute to standard development, encourage best design practices, and advance the DC value proposition. This work contributes by developing a novel framework of energy and power quality metrics and M&V methods, including:

- Simple but comprehensive metrics for the full-building electrical efficiency and power quality
- A measurement-informed modeling (MIM) method for calculating the electrical energy and efficiency of a building from the building's metered data
- A new voltage quality index (VQI) that characterizes a building's power quality and applies to both AC and DC buildings
- Guidelines for measuring a building's energy and power quality with an emphasis on affordable equipment and instrumentation.

This M&V framework will most benefit building operators and electrical system designers. Building operators often wish to be aware of their buildings' energy flows and power quality to reduce the electricity bill and prevent electrical problems. Electrical designers can use this framework to study various buildings and electrical topologies to develop best practices.

This work extends previous research on M&V procedures for calculating efficiency and loss [40]. The past work introduces energy metrics, the MIM method, and energy metering equipment. This

work augments the literature review and introduces the metrics, methods, and equipment necessary to measure power quality. In Section 2, this paper discusses the full-building efficiency metric and the MIM method for calculating loss. Section 3 introduces the proposed power quality metrics and explains their calculation. Section 4 describes the equipment and instrumentation required for measuring energy and power quality. Finally, these methods are experimentally applied at several sites, as described in Section 5.

2. Energy and Efficiency

2.1. Full-Building Efficiency Metric

Past research defines a variety of system-level energy metrics that can be useful in energy analytics and diagnosis [5]. This work recommends the scope be reduced to a single energy metric: full-building efficiency [6]. This simplification aims to allow a nontechnical audience to easily compare electrical loss between buildings.

For an electrical system, the full-building efficiency is:

$$\eta = 1 - \frac{E_{Loss}}{E_{Loss} + E_{Load}}, \tag{1}$$

where E_{Loss} is the electrical energy lost and E_{Load} is the total load energy consumed over a set period of performance.

2.2. Measurement-Informed Modeling Method

To completely determine E_{Loss} and E_{Load}, the user must meter every single electrical node in the building. Of course this is impossible in most buildings, which have thousands of devices. This work instead develops a completely new M&V procedure: the measurement-informed modeling (MIM) method. The MIM method calculates power flows from a model of the building's electrical network. This model is calibrated and refined based on metered data throughout the building. Increasing the number of meters allows for a more accurate model.

Users can calculate the system's losses based on the meter location, as shown in Figure 1. The electrical regions in this network are categorized as either zones or branches. Electrical zones are completely enclosed by meters. Electrical branches are electrical regions that have a single upstream meter. In a building, it is often most convenient to meter each circuit of each breaker panel.

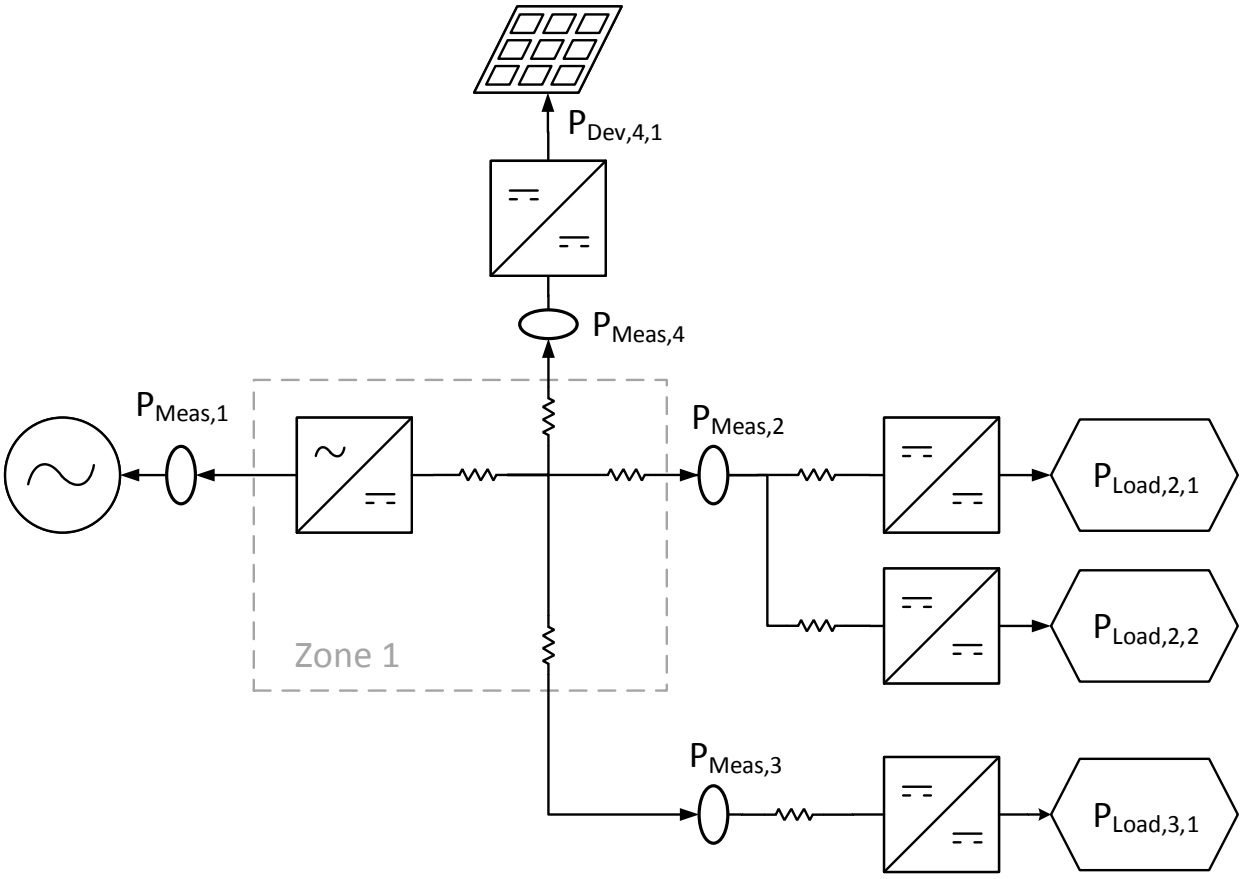

Figure 1: Example diagram for the MIM method

In AC systems, the meters only have to measure the active (real) power. This power should be calculated as the moving average of the product of the instantaneously-sampled voltage and current. As such, the MIM method is accurate even with bus-voltage distortion.

2.3. Zone Loss

If a zone is fully enclosed by meters, the MIM method can precisely calculate zone loss as a balance of power. The total loss in Zone z, $P_{LossZ,z}$ is calculated as:

$$P_{LossZ,z} = \left| \sum_{m \subseteq M} P_{Meas,m} \right|, \tag{2}$$

where $P_{Meas,m}$ is the power measured by meter m, and m is among the subset of meters enclosing zone z. In Figure 1, there is only one zone and $m = 1$ to 4. Equation (2) requires that the electrical zones only contain converters and wiring; loads, generation, or storage should all reside in metered branches. It is also important for the user to be consistent with the sign of $P_{Meas,m}$, which indicates direction of power flow relative to the meter's direction.

2.4. Branch Loss

Each meter measures the power, $P_{Meas,b}$, at branch b of a total B branches. For each branch b, the branch loss, $P_{Loss,b}$, is calculated as

$$P_{LossB,b} = \left| P_{Meas,b} - \sum_{d} P_{Dev,b,d} \right| \tag{3}$$

where $P_{Dev,b,d}$ is the power flowing into an electrical device d on branch b. For loads, $P_{Dev,b,d} = P_{Load,b,d}$ and is always positive. If the device is a grid connection, battery storage, or PV generation, $P_{Dev,b,d}$ can be positive or negative, depending on whether the device acts as a power sink or source, respectively.

Some devices can self-monitor and report their power flow. For most devices, however, the user must calculate $P_{Dev,b,d}$ based on $P_{Meas,b}$. They can accomplish this calculation by modeling the branch's converter and wire loss and back-solving for $P_{Dev,b,d}$. For example, $P_{Dev,3,1} = P_{Load,3,1}$ in Figure 1 can be determined from the wire loss $P_{Loss,w}$ and converter loss $P_{Loss,c}$ as:

$$P_{Dev,3,1} = P_{Meas,3} - P_{Loss,w,3} - P_{Loss,c,3}. \tag{4}$$

With appropriate knowledge or assumptions of the converter's efficiency curve, $\eta(P_{in})$, and wire resistance and RMS voltage, R_{wire} and V_{rms}, respectively, the losses can be approximately calculated as:

$$P_{Loss,w,3} = \frac{V_{rms}^2}{R_{wire}} \tag{5}$$

$$P_{Mid} = P_{Meas,3} - P_{Loss,w,3} \tag{6}$$

$$P_{Loss,c,3} = (1 - \eta(P_{Mid}))\, P_{Mid}. \tag{7}$$

Ideally, the converter efficiency curve is available in a datasheet and the wire resistance can be calculated based on a known length and gauge. However, without this data, the user must make modeling assumptions based on typical efficiency and wiring data for the given type of device. If multiple types of loads are present on the same branch (e.g., branch 2 in Figure 1), the user must make modeling assumptions about the distribution of power, which can be calculated from typical consumption profiles [41, 42].

2.5. Total Loss

After calculating the system losses, the user can aggregate the total loss, P_{Loss}, and total load, P_{Load}, as:

$$P_{Loss} = \sum_{b}^{B} P_{LossB,b} + \sum_{z}^{Z} P_{LossZ,z} \tag{8}$$

$$P_{Load} = \sum_{b}^{B} \sum_{d}^{D} P_{Load,b,d}. \tag{9}$$

They can determine the full-building efficiency via Equation (1), noting that:

$$E_{Loss} = T \sum_{k}^{K} P_{Loss}[k] \tag{10}$$

$$E_{Load} = T \sum_{k}^{K} P_{Load}[k], \tag{11}$$

where K is the number of samples in the period of performance and T is the sampling period in seconds.

2.6. Equivalent Building Models

The MIM method calculates the power profile, $P_{Dev,b,d}$, of each device in the system. This information allows the user to model an equivalent building with a different power distribution system. The building would have identical $P_{Dev,b,d}$ profiles but different converters and wiring. Most users would leverage this feature to compare a metered DC building with a modelled equivalent AC building. Losses in an AC building are usually dominated by AC/DC converters in the branch circuits. The losses in the AC/DC converters can be back-solved as:

$$P_{Loss} = \left(\frac{1}{\eta_{conv}^{-1}(P_{Dev,b,d})} - 1 \right) P_{Dev,b,d}, \tag{12}$$

with appropriate assumptions about the inverse converter efficiency curve, $\eta_{conv}^{-1}(P_{out})$.

3. Power Quality

As described in Section 1.3, this work develops power quality metrics that simplify the M&V process and apply equivalently to AC and DC systems. It recommends two metrics for power quality analysis: power factor and voltage quality index (VQI).

3.1. Power Factor

A building's (i.e. grid-tied microgrid's) power factor is measured at its point of common coupling, often by the utility meter. It is a measure of a system's power utilization and how much incoming power is reflected back to the grid and wasted. Its calculation is well understood as the product of the displacement factor and distortion factor. The building's power factor usually has no impact on its reliability or its ability to deliver power to its loads. However, this metric is highly relevant to the utility, and customers with poor power factors may be punished via increased electricity tariffs and charges.

3.2. Voltage Quality Index

The VQI is a completely new metric for the general quality of the microgrid or building's internal bus voltage over a specified period of performance. The VQI fully depicts the system's reliability and its ability to deliver power to the loads. This work develops a VQI based on three submetrics:

- M_{RMS}: A submetric based on the RMS voltage level, and accounts for short and long-duration sags, swells, and interruptions.
- M_{BAL}: A submetric that describes the bipolar or three-phase voltage unbalance.
- M_{WD}: A submetric for waveform distortion, which characterizes harmonics, interharmonics, notching, and AC coupling.

The submetrics can be considered individual scoring categories that each range from 0 to 1, similar to the power factor. They combine additively to calculate the VQI, M_{VQI}:

$$M_{VQI} = w_{RMS}M_{RMS} + w_{BAL}M_{BAL} + w_{WD}M_{WD}, \tag{13}$$

where each w_X is the proper weighting factor. The weights add to 1, and are assigned based on the perceived importance of each submetric, which may vary year-to-year depending on the state of the industry. Section 1.3 offers several methods from past research for calculating the weights; the focus of this section is on the submetrics themselves.

This work develops a VQI that is simple to understand and communicate among building and microgrid operators. The VQI can be measured, processed, and calculated using affordable equipment such as a micro-computer. In contrast, past power-quality indices only apply for either

AC or DC systems and often require attentive measurement with expensive instruments. This work's VQI is designed to use simple and quantitative calculations to give a general but accurate sense of an AC or DC system's power quality.

The VQI neglects several high-frequency power quality issues such as transients, which are expensive to measure and are usually reflected in the calculated submetrics anyway. For example, if a lightning strike causes a transient that disables the system, the resulting interruption is duly reflected in M_{RMS}. The VQI also excludes power quality issues related to the current. Although current measurements can be useful in diagnosis, the bus voltage ultimately determines how well the system powers the loads. Finally, the VQI excludes any submetrics related to flicker and frequency deviation. These power quality issues have traditionally been problematic in early LED drivers and fixed-speed synchronous motors. Nonetheless, flicker cancellation in LED drivers has drastically improved. In addition, most modern motors use variable-speed drives that are agnostic to the line frequency. As such, flicker and frequency deviation will soon become irrelevant and are thus excluded from the VQI.

Each VQI submetric is calculated every T seconds. These instantaneous submetric samples are averaged over a total of K samples during the period of performance. They are also averaged over the N measurement points in a system. Finally, each submetric's calculation is affected by an exponential penalty scalar, A_X, which determines how much to penalize poor performance. Like the weights, A_X may vary year to year.

3.3. RMS Voltage Submetric, M_{RMS}

The RMS voltage submetric, M_{RMS}, accounts for short- and long-duration sags, swells, and interruptions. These are among the most scrutinized power quality issues, as they can trigger lock-out mechanisms in loads and ultimately interrupt productivity. M_{RMS} is based on the instantaneous RMS voltage level, $v_{RMS}(t)$, which is calculated over a window of past samples of the bus voltage. This window should be at least 100 ms to include at least six 60 Hz cycles. The submetric's calculation compares $v_{RMS}(t)$ with the system's designated voltage tolerance band. The minimum RMS voltage, V_{min}, and maximum RMS voltage, V_{max}, may vary based on the chosen standard. For short-term effects greater than 100 ms, ITIC specifies a tolerance band between 0.9 and 1.1 p.u. [20]. Similarly, ANSI C84 specifies 114–126 V (i.e., 0.95–1.05 p.u.) for 120 V AC power distribution [21].

The normalized RMS error, $\epsilon_{rms}(t)$, is calculated as:

$$\epsilon_{rms}(t) = \begin{cases} (v_{rms}(t) - V_{max})/V_{nom} & v_{rms}(t) > V_{max} \\ (V_{min} - v_{rms}(t))/V_{nom} & v_{rms}(t) < V_{min} \\ 0 & V_{min} < v_{rms}(t) < V_{max} \end{cases}$$

where the absolute error is normalized by the nominal expected voltage value, V_{nom} (e.g. 120 V AC, 380 V DC, etc.). The instantaneous RMS submetric, $m_{RMS,n}(t)$, at measurement point n is

$$m_{RMS,n}(t) = 1 - \epsilon_{rms,n}(t). \tag{14}$$

M_{RMS} is ultimately calculated by averaging $m_{RMS,n}(t)$ over the N measurement points and K samples measured during the period of performance:

$$M_{RMS} = \left(\frac{1}{KN} \sum_{k=0}^{K} \sum_{n=0}^{N} m_{RMS,n}(kT) \right)^{A_{RMS}}, \tag{15}$$

where A_{RMS} is the penalty scalar assigned to the RMS submetric.

3.4. Unbalance Submetric, M_{BAL}

Unbalance can occur in multiphase or multipole systems with unmatched phase or pole voltages. It can cause wire transmission loss and overheating in transformers. Unbalance is quantified through the voltage unbalance factor F_{VU}. For three-phase AC,

$$F_{VU}(t) = \sqrt{\frac{1 - \sqrt{3 - 6\beta}}{1 + \sqrt{3 - 6\beta}}} \tag{16}$$

$$\beta = \frac{v_{ab}^4 + v_{bc}^4 + v_{ca}^4}{\left(v_{ab}^2 + v_{bc}^2 + v_{ca}^2\right)^2}, \tag{17}$$

given the phase-to-phase RMS voltages v_{ab}, v_{bc}, and v_{ca}. For bipolar DC or split-phase AC,

$$F_{VU}(t) = \left| \frac{v_p - v_n}{v_p + v_n} \right|, \tag{18}$$

where v_p and v_n are the RMS voltages on the positive and negative poles, respectively [25].

Similar to Section 3.3, the instantaneous voltage unbalance submetric, $m_{BAL,n}(t)$, is

$$m_{BAL,n}(t) = 1 - F_{VU}(t), \tag{19}$$

and the total voltage unbalance submetric, M_{BAL}, is

$$M_{BAL} = \left(\frac{1}{KN} \sum_{k=0}^{K} \sum_{n=0}^{N} m_{BAL,n}(kT) \right)^{A_{BAL}}. \tag{20}$$

In unipolar systems, $M_{BAL} = 1$.

3.5. Waveform Distortion Submetric, M_{WD}

Voltage waveform distortion introduces reactive currents that can increase loss and heat in the wiring, transformers, and filter capacitors of power supplies. It also creates electromagnetic noise that can disturb measurement or communication equipment. The most well-known waveform distortion metric is the total harmonic distortion (THD). However, AC and DC systems are both affected by interharmonics from switching power supplies. The waveform distortion submetric, M_{WD}, will have to account for both 60 Hz harmonics and interharmonics in the 10–100 kHz range. Although past works suggest the peak-to-peak ripple as an appropriate metric [25], peak measurements are highly vulnerable to noise.

This work recommends basing M_{WD} on the ripple distortion factor, F_{RD} [26]. F_{RD} is analogous to the THD but normalizes over all the spectral components, G_n, of the discrete Fourier transform (DFT):

$$F_{RD}(t) = \frac{1}{G_F}\sqrt{\sum_{n \neq F} G_n^2}. \tag{21}$$

This calculation normalizes each G_n by the fundamental component G_F. For DC, G_F is the nominal DC voltage, and the set of n should exclude the DC component. For AC, G_F is the 60 Hz fundamental, and the set of n should exclude the 60 Hz DFT component.

The DFT components are calculated via a fast Fourier transform (FFT) algorithm from a snapshot of time-series data. This work recommends recording time-series data over a 100 ms sampling window, which is six periods of 60 Hz or five periods of 50 Hz. An integral number of periods allows the FFT to avoid spectral leakage at the AC frequency, which is crucial for an accurate calculation of G_F. A 100 ms sampling window results in a precise DFT with 10 Hz frequency bins. This work also recommends a record length of at least 10,000 samples, which corresponds to a sampling rate of at least 100 kHz. Such a sampling rate can capture most major interharmonic frequencies, while still being easily attainable on affordable embedded computers.

Similar to Section 3.3, the calculation of M_{WD} follows as:

$$m_{WD,n}(t) = 1 - F_{RD}(t) \tag{22}$$

$$M_{WD} = \left(\frac{1}{KN}\sum_{k=0}^{K}\sum_{n=0}^{N} m_{WD,n}(kT)\right)^{A_{WD}}. \tag{23}$$

Table 1: Energy Measurement Equipment

Desired Quantity	**Available Equipment**
AC power	AC meter, multi-circuit meter
DC power	DC meter, integrated port monitoring
AC and DC voltage	Resistor divider, voltage transducer
AC current	Shunt, current transformer
DC current	Shunt, Hall-effect current sensor

4. Equipment and Instrumentation

This section reviews and categorizes the equipment available to measure energy and power quality. Although this section describes several high-end solutions, it also details affordable measurement methods that utilize assorted lab equipment.

4.1. Energy Measurement

Measuring the power through an electrical node generally requires the instantaneous measurement and multiplication of the node's current and voltage. Table 1 categorizes the different equipment available for the measurement of voltage, current, and power in AC and DC systems. Because AC metering and current transformers (CTs) are well understood, this subsection focuses on DC measurement techniques.

AC power meters are commonplace and can range in cost depending on functionality. At the high end, revenue-grade meters at the point of common coupling require revenue-grade CTs with less than 0.5% error. Home energy systems often use multi-circuit meters, whose multiple CTs can simultaneously meter every circuit in a breaker panel.

Of the DC metering solutions, the most accurate is a DC meter (e.g. the AccuEnergy AcuDC meter in Figure 2). DC meters can often log and upload data to the cloud. Although they are sometimes equipped with internal current sensing, they often require external current-measuring equipment. These units vary in cost, but are generally too expensive for mass metering. Since

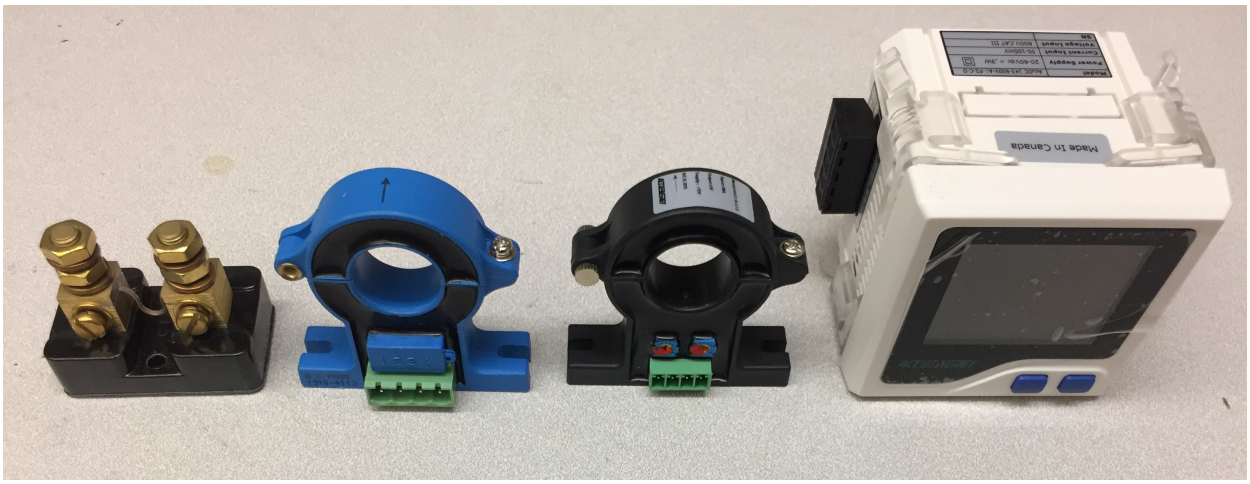

Figure 2: DC measurement equipment, including (right to left) a DC power meter, two hall-effect current transducers, and a current shunt

the MIM method encourages mass metering, the rest of this section describes more affordable measurement alternatives.

In DC systems, it is usually possible to measure a node's current and voltage separately, and multiply them in post-processing. In contrast, AC meters require a simultaneous measurement and multiplication, since simply multiplying the RMS voltage and current will not account for the power factor. In a DC system, current and voltage can be measured separately as long as the system satisfies the following requirements:

- The DC bus voltage is stable and approximately constant at the sampling/averaging time scale.
- The measured current must not regularly cross zero, i.e., it must actually be direct current.

Most functional DC systems will easily meet these conditions.

Voltage and current data can be aggregated, stored, and uploaded by a data logger. The typical practice is to install the logger within a breaker panel, along with a single bus voltage sensor and a current sensor for each circuit. Loggers such as the Campbell Scientific CR1000x or the Labjack both have many analog channels and networked capability.

The simplest and most affordable method of measuring voltage is through a precision resistor divider. However, this method is not galvanically isolated; it electrically couples the logger and the DC bus. Nonisolated methods may work for low-voltage systems (i.e., $\leq$ 48 V), though may also introduce a ground loop between the logger and the DC bus. As such, this work recommends

Table 2: Power Quality Measurement Equipment

Desired Quantity	**Available Equipment**
M_{WD}	Oscilloscope with differential voltage probe
M_{RMS}, M_{BAL}	An appropriate metering option from Table 1
Power factor	AC meter at the point of common coupling
Power quality diagnostics	Power quality or transient disturbance analyzer

an isolated voltage transducer for both low- and high-voltage solutions.

Installers can measure DC current using current shunts or hall-effect sensors, shown in Figure 2. Shunts are extremely precise resistors with a measurable voltage drop. They are more accurate than hall-effect sensors, and are recommended for low-current measurement ($\leq$ 10 A). However, shunts can be problematic due to their lack of galvanic isolation and resistive loss at high power. Shunts may incur higher installation time and cost due to their inline characteristics.

Hall-effect sensors sense current via the Hall effect: a current-carrying wire generates a measurable magnetic field. The most accurate hall-effect sensors are board-mount or on-chip solutions. However, field testing generally requires the convenience of the magnetic clamp-on hall-effect transducers in Figure 2. Clamp-on hall sensors may require extensive calibration, as their output varies with the tightness of the clamp and the ambient temperature. They also lose accuracy measuring below 20% rated current, and are thus recommended only for high-current applications.

Power distribution electronics with integrated power monitoring offer the most convenient method of measurement. A common trend in industry is to manage power distribution through the use of DC power servers. Power servers monitor the current and voltage at each of their outputs. They generally use accurate board-mounted measurement devices such as on-chip hall-effect sensors, shunts, and precision resistor dividers. The authors recommend self-monitoring and reporting for all power distribution electronics.

4.2. Power Quality Measurement

Building energy stakeholders are always seeking reliable but economical options to ensure sufficient power quality at a reasonable expense. Table 2 categorizes several instrumentation options for monitoring power quality. The metering equipment and techniques of Section 4.1 are sufficient to measure some of the submetrics in Section 3. However, other metrics such as waveform distortion may require high-frequency measurement, sampling, and data processing. Any type of power quality diagnostics will also require more intricate instrumentation such as oscilloscopes, power quality analyzers, and transient-disturbance analyzers.

Power quality analyzers can detect power delivery issues such as transients, voltage sags or swells, unbalance, flicker, and harmonics. They typically monitor voltage, current, and frequency, and also measure phase angle, power factor, balance, total harmonic distortion to gauge the overall quality of power. Some analyzers are fast enough to identify high-speed disturbance events such as faults, lightning strikes, ground loops, and common mode electrical noise. In general, high-frequency analysis requires a sampling frequency greater than twice the highest frequency of interest, according to the Nyquist criteria. Extensive fault analysis may also require some degree of protection, depending on the analyzer.

Transient-disturbance analyzers such as the P-Qube from Power Standards Lab are specifically designed to capture and report short-duration transients. Their exceptionally high sampling frequency allows for very accurate measurement of amplitude and frequency content. The amplitude of a disturbance is relevant to equipment damage, whereas the frequency may cause unwanted coupling to other circuits. Transient-disturbance analyzers must use short probe cables to avoid attenuation of high-frequency transients.

Power quality and transient disturbance analyzers can be prohibitively expensive in many M&V applications. An oscilloscope is often sufficient to measure the VQI from Section 3. Affordable oscilloscopes are easily available with the sampling rate and record lengths specified in Section 3. Any type of voltage measurement should use an appropriately rated differential or isolated probe to avoid hazardous ground loops. Current measurements should use a high-frequency clamp-on current probe. In general, the use of oscilloscopes requires manual operation and specialized M&V expertise.

Long-term power quality M&V studies would benefit from the availability of an affordable plug-

and-play power quality analyzer. The VQI from Section 3 is designed to have a light computational burden; it could be implemented on a Raspberry Pi. Such an affordable plug-and-play solution will ultimately be necessary if power quality is ever to become a central metric for comparing building power distribution networks.

5. Experimental Results

This work validates the feasibility of the M&V procedures through a series of experimental bench and field tests. The experiments each measure the site's energy efficiency and/or power quality:

- Laboratory bench test (AC distribution)—power quality
- Institute of Building Research (IBR) DC demonstration lab—energy and power quality
- IBR DC office building, 7th floor—energy.

Sections 5.1 to 5.3 describe each experiment and summarize key findings. These experiments are intended for demonstration and validation purposes, and so their duration is considerably shorter than an ideal M&V period of performance.

5.1. Laboratory Bench Test

The first experiment validates the feasibility of measuring and calculating the VQI metric in AC systems. Its voltage data are measured from a lab wall outlet at Lawrence Berkeley National Laboratory. Since the lab operates on single-phase AC distribution, $M_{BAL} = 1$ and only one measurement point is necessary.

This experiment used a Chroma 66202 power meter to measure the RMS voltage every second (10 Hz sampling would have been better) for a total duration of 1 hour. During this time, the RMS bus voltage varied between 120.32 V and 122.31 V, which is well within the ANSI C84.1 limits of 114–126 V. There was also a simulated 2-minute blackout at the 10-minute mark, during which the RMS bus voltage was zero. With a penalty scalar of $A_{RMS} = 10$, the resulting RMS submetric is $M_{RMS} = 0.711$.

The ratio between blackout and up-time in this experiment is equivalent to 12 days of blackout per year. Although this seems high, it is fairly realistic for California communities affected by public safety power shutoffs during fire season. Islands and developing countries experience even

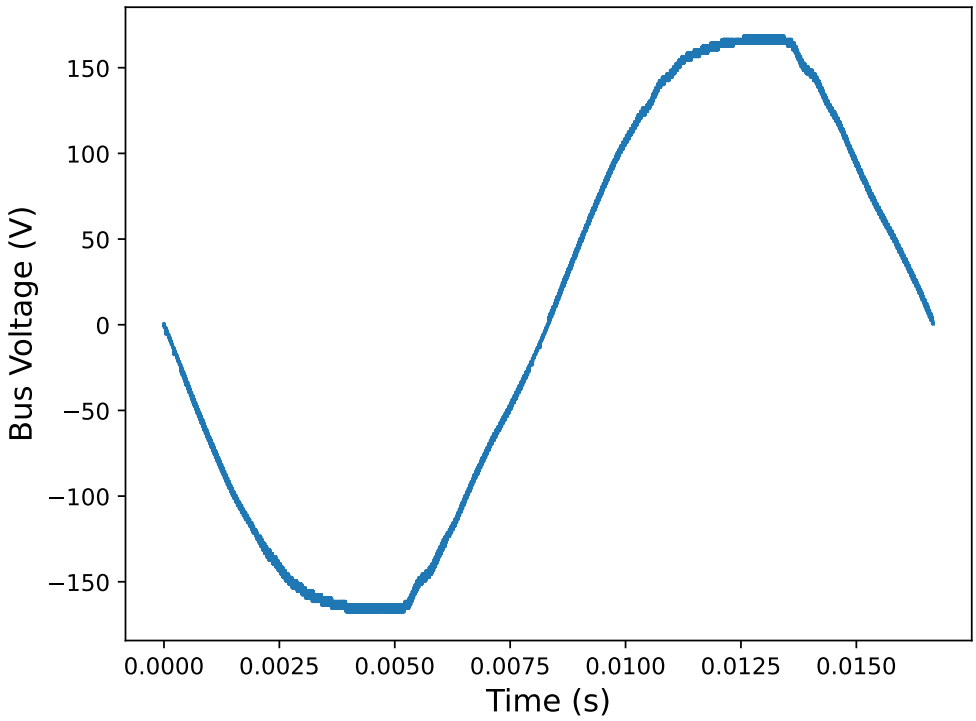

Figure 3: One period of the AC waveform in the lab

longer and more sporadic blackouts. As such, $A_{RMS} = 10$ may well be the appropriate penalty scalar, depending on whatever becomes the standard for good power quality.

To measure waveform distortion, this experiment used a Sigilent SDS1104X-E oscilloscope, which has a record length of 14 million. The voltage was measured from the wall using a Cal-test Electronics CT4068 differential probe. The voltage waveform, shown in Figure 3, is slightly distorted. With a penalty scalar of $A_{WD} = 2$, the resulting waveform distortion submetric is $M_{WD} = 0.940$. This essentially means the bus voltage is 94% sinusoidal, which is appropriate for the level of distortion in Figure 3.

5.2. Institute of Building Research DC Demonstration Lab

The DC Demonstration Lab is part of the Institute of Building Research (IBR) Low Carbon City campus on the outskirts of Shenzhen, China. This lab, pictured in Figure 4, functions to demonstrate IBR's DC building research. It contains a small DC microgrid, which connects the grid-tie inverters, storage, PV generation, and HVAC on a 540 V DC bus. The system powers its other DC loads at 220 V, 24 V, and 5 V, including lighting, displays, and multiple small-scale demonstration experiments.

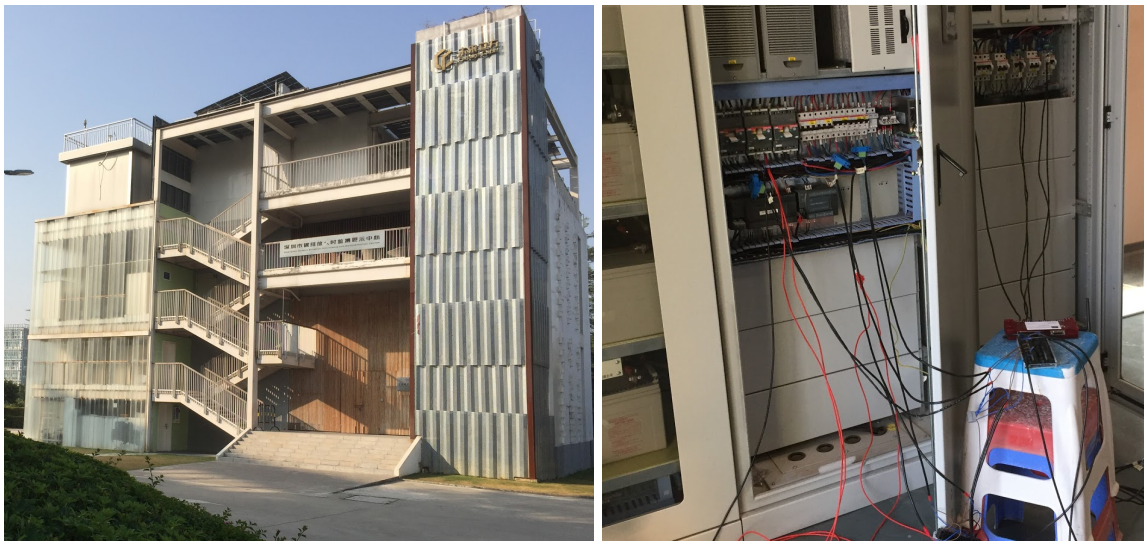

Figure 4: The IBR DC Lab is on the first floor (left). The metering prototype is set up within the electrical cabinet (right).

The authors metered the system using resistor dividers and YHDC 50 A clamp-on hall-effect sensors. The Labjack T7 Pro data logger easily metered the eight current and three voltage measurement points within the electrical cabinet, shown in Figure 4. The YHDC sensors were somewhat oversized for the system's typical current and had to be calibrated manually. The authors used a precision resistor divider to measure the voltage level of each power distribution bus (540 V, 220 V, 24 V, 5 V). While accurate, this approach required the authors to carefully confirm the absence of ground loops.

The authors analyze the system's energy and efficiency in both grid-tied and islanded operation. The full-building efficiency of each ten-minute experiment is shown in Table 3. The system was 87.1% efficient in grid-tied operation and 89.9% efficient in islanded operation.

The building model generates a loss breakdown, which reveals the power converters and fans in the electrical cabinet zone to contribute the most system loss. As shown in Table 3, the electrical cabinet comprised 68% of the loss in the grid-tied experiment and 88% of the loss in the islanded experiment. The electrical cabinet was oversized for the IBR DC Lab's requirements, likely to allow for expansion in the future. Power converters are usually less efficient when operating at low capacity. It is generally important for the converters to be sized appropriately for the system requirements.

Another problem was the over-use of converters within the electrical cabinet. There are three conversion stages between the 540 V bus and the 24 V bus. Such a design was likely motivated

Table 3: IBR DC Lab Efficiency and Loss

Source of Loss	**Grid-Tied Experiment**	**Islanded Experiment**
All load branches (Wh)	8.4	8.1
Grid-tied inverter branch (Wh)	26.9	1.1
Electrical cabinet zone (Wh)	75.6	70.4
Total load (Wh)	747.7	706.5
Total loss (Wh)	111.0	79.6
System efficiency	87.1%	89.9%

by the lack of off-the-shelf converters at the appropriate voltage levels. While this design may be acceptable for a demonstration, the industry will ultimately need a single highly-efficient converter between the high-voltage and low-voltage busses.

For this exercise, the authors use the 220 V bus to sample and calculate the RMS and waveform distortion submetrics. The RMS submetric can leverage the bus voltage data from the energy experiments, which has a sampling rate of 1 Hz. The bus voltage ranges between 220.5 V and 223.1 V, which is easily within the 5% tolerance band (209–231 V). As such, $M_{RMS} = 1.0$ over the 10-minute period of performance for both the grid-connected and the islanded experiments.

For waveform distortion, the only equipment available on-site was a Hantek 2C42 oscilloscope with a record length of 1,200. Although 1,200 samples is not nearly high enough to capture typical power switching frequencies, it is sufficient for validation purposes. As shown in Figure 5, the 220 V DC bus waveform was relatively clean, which is expected for the output of the 540 V to 220 V converter. The waveform distortion submetric is $M_{WD} = 0.992$.

Figure 5 shows a bus-voltage waveform with several transient spikes, which can increase the peak-to-peak ripple. While M_{WD} does capture these spikes, they are ultimately averaged out with the rest of the FFT components. M_{WD} is not intended to analyze individual peaks or transients, but rather to report the overall waveform distortion. If the analyst suspects that transient spikes are of sufficient concern, they should use a specialized power quality or transient disturbance analyzer.

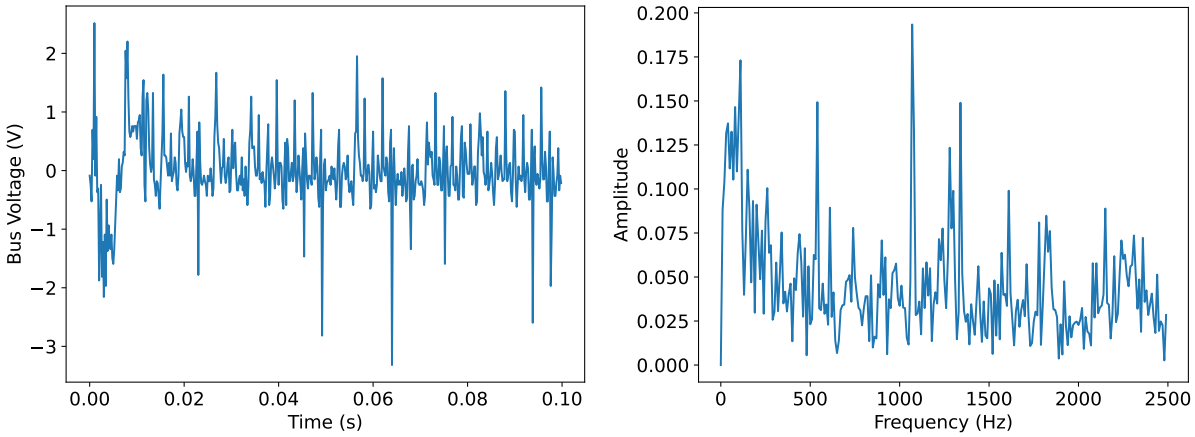

Figure 5: A snapshot of the AC content of the 220 V DC bus waveform (left) and its FFT (right)

Figure 6: The eight-floor IBR DC office building, still under construction (left). IBR's power distribution box for 48 V distribution over each floor (right).

5.3. IBR DC Office Building

Over 95% of the loads in IBR's new DC office building take a direct-DC input. This recently built installation, shown in Figure 6, features one of the world's first loosely-coupled bipolar DC distribution systems. Its +/- 375 V bus couples a 150 kW PV array and 100 kWh battery bank to the DC loads. Its high-voltage loads include several 750 V DC EV chargers and air conditioners. Six of the eight floors are designated as office space, each of these floors has ten controllable power distribution boxes. These boxes convert 375 V to 48 V at 95% efficiency and precisely control the 48 V power distribution to the plug loads, fans, and lighting. The boxes each contain 1 kWh of distributed storage to assist with localized resiliency and peak shaving. This field test leverages the capability of each box to precisely measure and report the power at each of its 48 V output ports.

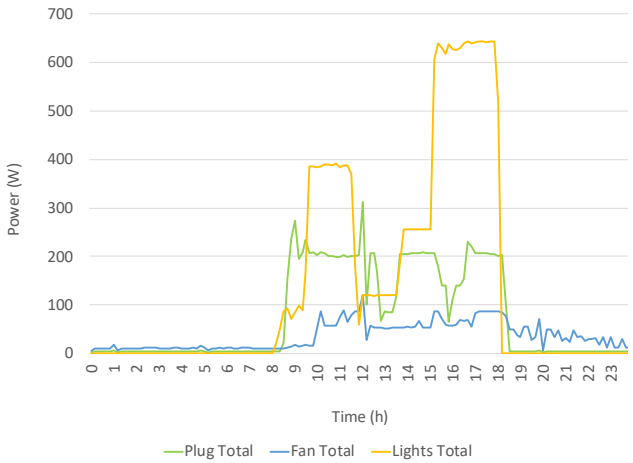

Figure 7: The aggregate load profile, sorted by load category, of the IBR DC office building's seventh floor

The field test studied the losses on the seventh floor over a day. The categorized load profile shown in Figure 7 indicates a low occupancy. Table 4 presents the full-floor efficiency: 92.6%. A modelled equivalent AC building has a slightly lower efficiency of 90.9%. The DC network has relatively low power-conversion loss in the load branches. Its losses in the load-packaged converters and branch wiring are 29% that of the AC network. However, the internal power conversions in each power distribution box contribute 64% of the DC-network loss. Although the boxes offer control, storage, and energy reporting, these benefits come at a slight cost in efficiency. There are many emerging point-to-point DC topologies that emphasize controllability and managed power as a selling point. The results of this study may well have energy implications for managed DC topologies. Further study on other buildings can reveal whether the controllability benefits of managed DC outweigh the energy benefits of bus-based DC topologies.

6. Conclusion and Future Work

At this stage, the DC microgrid industry desperately needs simple and effective metrics of comparison. This work establishes the full-building efficiency metric, which it calculates using a new measurement-informed modeling (MIM) method. The MIM method constructs an electrical model of the building, which it refines with live metered data. This research also develops a new type of power quality index that can apply to DC systems and is simple and affordable to measure. The voltage quality index is an aggregate metric based on the voltage level, unbalance, and waveform distortion. This work shows how the energy and power quality metrics can be measured through a series of field experiments, which validate the overall feasibility of the measurement and verification

Table 4: Efficiency and Loss of the IBR DC Office Building

Source of Loss	**IBR DC Office Building**	**Equivalent AC Building**
All load branches (Wh)	177	612
All box zones (Wh)	316	0
Total load (Wh)	6143	6143
Total loss (Wh)	493	612
System efficiency	92.6%	90.9%

(M&V) procedures.

Future work includes the refinement of the energy and power quality metrics and methodology, and would require careful study and review by multiple experts. Should these metrics be accepted among the academic community, it will be necessary to develop standards and educate developers and electricians. Beyond energy and power quality, additional M&V procedures must be established to study and compare the cost, safety, and reliability between DC and AC buildings. In addition, further research should individually assess the value of features specific to DC microgrids, including managed power distribution, distributed storage, and combined data and power.

Acknowledgements

The authors are grateful for their colleagues at the Institute of Building Research for their assistance in data collection. Special thanks to Jing Kang, Wenyu Pan, and Yutong Li for their kind support.

This research was developed jointly by Lawrence Berkeley National Laboratory, operated for the U.S. Department of Energy (DOE) under Contract No. DE-AC02-05CH11231, and also the National Renewable Energy Laboratory, operated by Alliance for Sustainable Energy, LLC, for the DOE under Contract No. DE-AC36-08GO28308. Funding was provided by the DOE Assistant Secretary for Energy Efficiency and Renewable Energy Building Technologies Office Emerging Technologies Program. The views expressed in the article do not necessarily represent the views

of the DOE or the U.S. Government.

Finally, the authors extend thanks to the rest of the DC team and partners, all of whom work hard to further the DC industry.

References

[1] S. Backhaus, G. W. Swift, S. Chatzivasileiadis, W. Tschudi, S. Glover, M. Starke, J. Wang, M. Yue, D. Hammerstrom, DC Microgrids Scoping Study Estimate of Technical and Economic Benefits, Tech. Rep. LA-UR-15-22097, Los Alamos National Laboratory (Mar. 2015).

[2] P. Savage, R. R. Nordhaus, S. P. Jamieson, From Silos to Systems: Issues in Clean Energy and Climate Change: DC microgrids: benefits and barriers, Tech. rep., Yale School of Forestry & Environmental Sciences (2010).

[3] V. Vossos, K. Garbesi, H. Shen, Energy savings from direct-DC in U.S. residential buildings, Energy and Buildings 68, Part A (2014) 223–231. doi:10.1016/j.enbuild.2013.09.009.
URL http://www.sciencedirect.com/science/article/pii/S0378778813005720

[4] S. M. Frank, S. Rebennack, Optimal design of mixed AC-DC distribution systems for commercial buildings: A nonconvex generalized benders decomposition approach, European Journal of Operational Research 242 (3) (2015) 710 – 729. doi:https://doi.org/10.1016/j.ejor.2014.10.008.
URL http://www.sciencedirect.com/science/article/pii/S0377221714008121

[5] D. Fregosi, S. Ravula, D. Brhlik, J. Saussele, S. Frank, E. Bonnema, J. Scheib, E. Wilson, A comparative study of DC and AC microgrids in commercial buildings across different climates and operating profiles, in: 2015 IEEE First International Conference on DC Microgrids (ICDCM), 2015, pp. 159–164. doi:10.1109/ICDCM.2015.7152031.

[6] D. L. Gerber, V. Vossos, W. Feng, C. Marnay, B. Nordman, R. Brown, A simulation-based efficiency comparison of AC and DC power distribution networks in commercial buildings, Applied Energy 210 (2018) 1167 – 1187. doi:https://doi.org/10.1016/j.apenergy.2017.05.179.
URL http://www.sciencedirect.com/science/article/pii/S0306261917307419

[7] P. Ollas, Energy savings using a direct current distribution network in a PV and battery equipped residential building, Ph.D. thesis (03 2020).

[8] F. W. Y. Saputra, Aripriharta, I. Fadlika, N. Mufti, K. H. Wibowo, G. J. Jong, Efficiency comparison between DC and AC grid toward green energy in Indonesia, in: 2019 IEEE International Conference on Automatic Control and Intelligent Systems (I2CACIS), 2019, pp. 129–134. doi:10.1109/I2CACIS.2019.8825014.

[9] H. E. Gelani, F. Dastgeer, K. Siraj, M. Nasir, K. A. K. Niazi, Y. Yang, Efficiency comparison of AC and DC distribution networks for modern residential localities, Applied Sciences 9 (3) (2019). doi:10.3390/app9030582.
URL https://www.mdpi.com/2076-3417/9/3/582

[10] F. Dastgeer, H. E. Gelani, A comparative analysis of system efficiency for AC and DC residential power distribution paradigms, Energy and Buildings 138 (2017) 648–654. doi:https://doi.org/10.1016/j.enbuild.2016.12.077.
URL https://www.sciencedirect.com/science/article/pii/S0378778816320461

[11] K. Siraj, H. A. Khan, DC distribution for residential power networks a framework to analyze the impact of voltage levels on energy efficiency, Energy Reports 6 (2020) 944–951. doi:https://doi.org/10.1016/j.egyr.2020.04.018.
URL https://www.sciencedirect.com/science/article/pii/S2352484719313757

[12] H. E. Gelani, F. Dastgeer, M. Nasir, S. Khan, J. M. Guerrero, AC vs. DC distribution efficiency: Are we on the right path?, Energies 14 (13) (2021). doi:10.3390/en14134039.
URL https://www.mdpi.com/1996-1073/14/13/4039

[13] D. L. Gerber, F. Musavi, O. A. Ghatpande, S. M. Frank, J. Poon, R. E. Brown, W. Feng, A comprehensive loss model and comparison of AC and DC boost converters, Energies 14 (11) (2021). doi:10.3390/en14113131.
URL https://www.mdpi.com/1996-1073/14/11/3131

[14] D. L. Gerber, R. Liou, R. Brown, Energy-saving opportunities of direct-DC loads in buildings, Applied Energy 248 (2019) 274–287. doi:https://doi.org/10.1016/j.apenergy.2019.04.089.
URL https://www.sciencedirect.com/science/article/pii/S0306261919307470

[15] A. Stippich, A. Sewergin, G. Engelmann, J. Gottschlich, M. Neubert, C. van der Broeck, P. Schuelting, R. Goldbeck, R. De Doncker, From ac to dc: Benefits in household appliances, in: International ETG Congress 2017; Proceedings of, VDE, 2017, pp. 1–6.

[16] A. H. Sabry, A. H. Shallal, H. S. Hameed, P. J. Ker, Compatibility of household appliances with DC microgrid

for PV systems, Heliyon 6 (12) (2020) e05699. doi:https://doi.org/10.1016/j.heliyon.2020.e05699.
URL https://www.sciencedirect.com/science/article/pii/S2405844020325421
[17] U. Boeke, M. Wendt, DC power grids for buildings, in: 2015 IEEE First International Conference on DC Microgrids (ICDCM), 2015, pp. 210–214. doi:10.1109/ICDCM.2015.7152040.
[18] IEEE recommended practice for monitoring electric power quality, IEEE Std 1159-2019 (Revision of IEEE Std 1159-2009) (2019) 1–98doi:10.1109/IEEESTD.2019.8796486.
[19] H. Markiewicz, A. Klajn, Voltage disturbances standard en 50160 - voltage characteristics in public distribution systems, 2008.
[20] IEEE recommended practice for emergency and standby power systems for industrial and commercial applications, IEEE Std 446-1995 [The Orange Book] (1996) 1–320doi:10.1109/IEEESTD.1996.85950.
[21] American national standard for electric power systems and equipment—voltage ratings (60 hertz), ANSI C84.1-2011 (2011).
[22] IEEE recommended practice and requirements for harmonic control in electric power systems, IEEE Std 519-2014 (2014).
[23] Electromagnetic compatibility (emc) - part 3-2: Limits - limits for harmonic current emissions (equipment input current 16 a per phase), IEC 61000-3-2:2018 (2018).
[24] Electromagnetic compatibility (emc) - part 3-3: Limits - limitation of voltage changes, voltage fluctuations and flicker in public low-voltage supply systems, for equipment with rated current 16 a per phase and not subject to conditional connection, IEC 61000-3-3:2013 (2013).
[25] G. Van den Broeck, J. Stuyts, J. Driesen, A critical review of power quality standards and definitions applied to DC microgrids, Applied Energy 229 (2018) 281–288. doi:10.1016/j.apenergy.2018.07.058.
[26] J. Barros, M. de Apr˚iz, R. I. Diego, Power quality in DC distribution networks, Energies 12 (5) (2019). doi:10.3390/en12050848.
URL https://www.mdpi.com/1996-1073/12/5/848
[27] S. Whaite, B. Grainger, A. Kwasinski, Power quality in DC power distribution systems and microgrids, Energies 8 (5) (2015) 4378–4399. doi:10.3390/en8054378.
URL https://www.mdpi.com/1996-1073/8/5/4378
[28] V. Gosbell, B. Perera, H. Herath, Unified power quality index (UPQI) for continuous disturbances, in: 10th International Conference on Harmonics and Quality of Power. Proceedings (Cat. No. 02EX630), Vol. 1, IEEE, 2002, pp. 316–321.
[29] H. C. Herath, V. J. Gosbell, S. Perera, Power quality (PQ) survey reporting: discrete disturbance limits, IEEE transactions on power delivery 20 (2) (2005) 851–858.
[30] G. Carpinelli, P. Caramia, P. Varilone, P. Verde, R. Chiumeo, I. Mastrandrea, F. Tarsia, O. Ornago, A global index for discrete voltage disturbances, in: 2007 9th International Conference on Electrical Power Quality and Utilisation, IEEE, 2007, pp. 1–5.
[31] B. Lee, K. M. Kim, Unified power quality index based on value-based methodology, in: 2009 IEEE Power & Energy Society General Meeting, IEEE, 2009, pp. 1–8.
[32] B. Lee, K. M. Kim, Y. Goh, Unified power quality index using ideal AHP, in: 2008 13th International Conference on Harmonics and Quality of Power, IEEE, 2008, pp. 1–5.
[33] P. Langouranis, S. Kaminaris, G. Vokas, T. Raptis, G. C. Ioannidis, Fuzzy total power quality index for electric networks, in: MedPower 2014, IET, 2014, pp. 1–6.
[34] G. S. Elbasuony, S. H. A. Aleem, A. M. Ibrahim, A. M. Sharaf, A unified index for power quality evaluation in distributed generation systems, Energy 149 (2018) 607–622.
[35] G. R. de Castro, V. B. Riboldi, T. Ji, X. Chen, Unified power quality index method using AHP for consumers sensitivity evaluation, in: 2020 IEEE PES Transmission & Distribution Conference and Exhibition-Latin America (T&D LA), IEEE, pp. 1–6.
[36] H. Sindi, E. El-Saadany, Unified reliability index development for utility performance assessment, Intelligent Industrial Systems 2 (2) (2016) 149–161.
[37] M. Jasiński, T. Sikorski, P. Kostyła, Z. Leonowicz, K. Borkowski, Combined cluster analysis and global power quality indices for the qualitative assessment of the time-varying condition of power quality in an electrical power network with distributed generation, Energies 13 (8) (2020) 2050.
[38] M. Sacasqui, J. Luyo, A. Delgado, A unified index for power quality assessment in distributed generation systems using grey clustering and entropy weight, in: 2018 IEEE ANDESCON, IEEE, 2018, pp. 1–4.
[39] T. Raptis, G. Vokas, P. Langouranis, S. Kaminaris, Total power quality index for electrical networks using neural networks, Energy Procedia 74 (2015) 1499–1507.
[40] D. L. Gerber, O. A. Ghatpande, M. Nazir, W. G. B. Heredia, W. Feng, R. Brown, Electrical measurement

and verification of energy in DC buildings, in: 2021 IEEE Fourth International Conference on DC Microgrids (ICDCM), 2021, pp. 1–6. doi:10.1109/ICDCM50975.2021.9504609.

[41] F. M. Orr, 2015 quadrennial technology review, in: Proceedings of the International Conference for High Performance Computing, Networking, Storage and Analysis, 2015.

[42] J. Butzbaugh, R. Hosbach, A. Meier, Miscellaneous electric loads: Characterization and energy savings potential, Energy and Buildings 241 (2021) 110892. doi:https://doi.org/10.1016/j.enbuild.2021.110892.
URL https://www.sciencedirect.com/science/article/pii/S0378778821001766